Microwave dynamics of the stoichiometric and bond-disordered anisotropic $S = 1$ chain antiferromagnet $NiCl_2$-4SC$(NH_2)_2$

T. A. Soldatov,[1,2] A. I. Smirnov,[1,3] K. Yu. Povarov,[4] A. Paduan-Filho,[5] and A. Zheludev[4]

[1]*P. L. Kapitza Institute for Physical Problems, RAS, 119334 Moscow, Russia*
[2]*Moscow Institute for Physics and Technology, 141701 Dolgoprudnyi, Russia*
[3]*National Research University Higher School of Economics, 101000 Moscow, Russia*
[4]*Laboratory for Solid State Physics, ETH Zürich, 8093 Zürich, Switzerland*
[5]*High Magnetic Field Laboratory, University of São Paulo, BR-05315-970 São Paulo, Brazil*

(Received 29 November 2019; revised manuscript received 20 February 2020; accepted 25 February 2020; published 9 March 2020)

We studied electron spin resonance in a quantum magnet $NiCl_2$-4SC$(NH_2)_2$, demonstrating a field-induced quantum phase transition from a quantum-disordered phase to an antiferromagnet. We observe two branches of the antiferromagnetic resonance of the ordered phase, one of them has a gap, and the other is a Goldstone mode with zero frequency at a magnetic field along the fourfold axis. This zero-frequency mode acquires a gap at a small tilting of the magnetic field with respect to this direction. The upper gap was found to be reduced in the Br-substituted compound $Ni(Cl_{1-x}Br_x)_2$-4SC$(NH_2)_2$ with $x = 0.21$. This reduction is unexpected because of the previously reported rise in the main exchange constant in a substituted compound. Furthermore, a nonresonant diamagnetic susceptibility χ' was found for the ordered phase in a wide frequency range above the quasi-Goldstone mode. This dynamic diamagnetism is as large as the dynamic susceptibility of the paramagnetic resonance. We speculate that it originates from a two-magnon absorption band of the low-frequency dispersive magnon branch.

DOI: 10.1103/PhysRevB.101.104410

I. INTRODUCTION

Antiferromagnetic spin $S = 1$ chains were intensively studied both theoretically and experimentally. Their peculiar features are quantum-disordered nonmagnetic ground states with an energy gap for magnetic excitations. The spin gap of collective excitations may have an exchange origin as the well-known Haldane gap [1] or, alternatively, may be due to the single-ion easy-plane anisotropy. The anisotropy makes the single-ion states with $S^z = 0$ preferable, preventing the magnetic ordering [2–4]. Although a lot of Haldane magnets were studied, quantum paramagnet ground states provided by strong anisotropy are not typical. $NiCl_2$-4SC$(NH_2)_2$ [dichloro-tetrakisthiourea-nickel(II), abbreviated as DTN] is a rare example of a spin system of this type. The low-temperature quantum-disordered state of DTN was found to be unstable in the magnetic-field $\mu_0 H_{c1} = 2.1$ T directed parallel to the fourfold axis c. In this field, a quantum phase transition into the antiferromagnetically ordered phase occurs [5]. At this transformation, the spin gap of excitations at the Brillouin-zone boundary is closing [6]. In the field range $H_{c1} < H < H_{c2}$, DTN is an antiferromagnet with magnon excitations. The antiferromagnetic state disappears upon heating above the Néel temperature T_N which has a maximum value of 1.2 K in the magnetic field near 7 T. At zero temperature, the values of the critical fields are $\mu_0 H_{c1} = 2.1$ and $\mu_0 H_{c2} = 12.6$ T [5,7–9]. The second critical field of the field-induced antiferromagnetic phase at $T = 0$ coincides with the field of magnetic saturation. At the temperature rise, both critical fields move to the middle of the interval, i.e., to 7 T and disappear above 1.2 K. The field-induced ordering in DTN was interpreted, in particular, in terms of Bose-Einstein condensation of magnons [9], although the validity of such an interpretation has been later questioned [10].

A quantum phase transition in DTN was recently shown to be induced not only by a magnetic field, but also by nonmagnetic Br substitution. Br ions substitute Cl ions, and this creates bond disorder via local variations of exchange and anisotropy parameters. Zero-field neutron-scattering experiments [11–14] reveal a decrease in the spin excitation gap at the boundary of the Brillouin zone for $Ni(Cl_{1-x}Br_x)_2$-4SC$(NH_2)_2$ (DTNX). This gap is completely closed at $x \simeq 0.16$ [12–14]. At $x = 0.21$, the antiferromagnetic long-range order appears even at the zero field at $T_N = 0.64$ K [13].

The Bose-Einstein scenario and the easy-plane antiferromagnetic ordering itself should result in a gapless Goldstone mode in a field $\boldsymbol{H} \parallel c$ [9,15]. A low-frequency electron spin resonance (ESR) mode was, indeed, observed in the ordered phase in addition to a higher resonance branch as described in Ref. [15]. However, because of the nonzero frequency, the low-frequency resonance mode was interpreted as an exchange mode with antiphase oscillations of two interpenetrating tetragonal subsystems. At the same time, a Goldstone mode was assumed to have a zero frequency and to remain invisible. The unusual low-frequency mode as well as the essential influence of nonmagnetic impurities on the spin excitations spectra, found in neutron-scattering experiments, motivated us to perform a detailed ESR investigation at a wider frequency range, different orientations of the magnetic field, and different substitution concentrations. In the present

paper, we find that the previously observed low-frequency antiferromagnetic resonance (AFMR) mode appears at a finite frequency due to a small tilting of magnetic field with respect to the c axis. This breaks the fourfold axis symmetry and, hence, results in the gap for the quasi-Goldstone mode. This mode drops to zero frequency at the precise orientation. Thereby the two-branch AFMR spectrum with a gapped mode and a true Goldstone mode is experimentally confirmed. The upper gap of the AFMR was found to be reduced in the Br-substituted sample with $x = 0.21$, despite the rise in the exchange integral near Br impurity [16] and the widening of the magnon band [14].

In addition, our measurements of the microwave magnetic responses both in DTN and in DTNX reveal an unusual nonresonant dynamic magnetic susceptibility of a diamagnetic type. This dynamic diamagnetism appeared in a wide frequency range with a lower boundary at a quasi-Goldstone mode. This nonresonant response may indicate a band of two-magnon microwave absorption. The width of this band corresponds to the dispersion range of the lower magnon branch.

II. CRYSTAL STRUCTURE AND MAGNETIC PARAMETERS OF DTN

The crystals of DTN belong to the $I4$ tetragonal space group [17]. Lattice parameters are $a = 9.558$ and $c = 8.981$ Å. Magnetic ions Ni^{2+} carrying spin $S = 1$ are placed on a body-centered tetragonal lattice consisting of two interpenetrating tetragonal sublattices. The sublattices are shifted relative to one another along the spatial diagonal of the tetragonal unit cell by half of its diagonal length.

Each sublattice represents a spin subsystem with antiferromagnetic exchange. For the whole spin system, the model Hamiltonian at the magnetic field parallel to the c axis can be written as follows:

$$\begin{aligned}\mathcal{H} = &\frac{1}{2}\sum_{\boldsymbol{m},\boldsymbol{\delta}} J_{\boldsymbol{\delta}} \boldsymbol{S_m}\cdot\boldsymbol{S_{m+\delta}} + \sum_{\boldsymbol{m}}\left[D\left(S^z_{\boldsymbol{m}}\right)^2 + g_c\mu_B H S^z_{\boldsymbol{m}}\right]\\ &+\frac{1}{2}\sum_{\boldsymbol{n},\boldsymbol{\delta}} J_{\boldsymbol{\delta}} \boldsymbol{S_n}\cdot\boldsymbol{S_{n+\delta}} + \sum_{\boldsymbol{n}}\left[D\left(S^z_{\boldsymbol{n}}\right)^2 + g_c\mu_B H S^z_{\boldsymbol{n}}\right]\\ &+\mathcal{H}_{\rm int},\end{aligned} \tag{1}$$

where $\boldsymbol{S_{m,n}}$ are spin-1 operators at sites $\boldsymbol{m}$, $\boldsymbol{n}$ belonging to the first and second subsystems, correspondingly, the vectors $\boldsymbol{\delta}$ connect the sites $\boldsymbol{m}$, $\boldsymbol{n}$ to their nearest neighbors within a subsystem, D is the easy-plane single-ion anisotropy constant, $J_{\boldsymbol{\delta}}$'s are the exchange constants, $g_c\mu_B H S^z_{\mathbf{n,m}}$'s are Zeeman terms, g_c is the corresponding g factor, and $\mathcal{H}_{\rm int}$ describes additional interactions, including the interaction between the subsystems.

The interaction between the subsystems is characterized by the exchange integral between the corner and the center cell ions J''. The exchange and anisotropy parameters were derived from the analysis of the excitation spectrum obtained in neutron-scattering experiments on fully polarized samples [6]: $D = 8.9$, $J_c = 2.05$, $J_{ab} = 0.156$, $J'' = 0.08$ K. These values agree with the earlier ESR study [18] which report all these parameters except for J''. The earlier neutron-scattering investigations [9] give close values of $D = 8.12$, $J_c = 1.74$, $J_{ab} = 0.17$ K. The intersubsystem exchange J'' is frustrated. The magnetic subsystems are, thus, decoupled at the zero field in the mean-field approximation.

III. EXPERIMENTAL DETAILS

Single-crystalline samples of DTN and DTNX used in our experiments are from the same batches as studied in previous ESR and neutron-scattering experiments [12–15,18]. Experimental results presented in Figs. 1–4 and Figs. 7–10 were obtained using the crystals synthesized in ETH Zürich and the results shown in Figs. 5, 6—for crystals grown at the University of São Paulo.

The ESR measurements were carried out with the use of a homemade transmission-type microwave spectrometer equipped with a superconducting 12-T magnet and a ^{3}He cryostat providing low temperatures down to 0.45 K. Cylindrical, rectangular, and cut-ring multimode resonators were used to cover a wide frequency range of 4–160 GHz. High-frequency 160–380-GHz measurements were performed with use of a cylindrical multimode resonator. Gunn diodes, backwave oscillators, and klystrons were used as microwave sources. Crystal samples were mounted inside the resonators, and a small amount of 2,2-diphenyl-1-picrylhydrazyl (DPPH) was placed near the sample as a standard $g = 2.00$ marker for the magnetic field. The sample size was chosen small enough not to disturb the electromagnetic field in a resonator. At the same time, the sample should be large enough to give the observable ESR signal. Thus, the crystals with the masses between 1 and 90 mg were used for measurements at different frequencies.

ESR absorption lines were recorded as field dependencies of the microwave power transmitted through the resonator. If the generator is tuned to resonator frequency $f_{\rm res}$, the transmitted signal is (see, e.g., Ref. [19]) as follows:

$$U = U_0/(1 + 4\pi\chi''\eta Q)^2, \tag{2}$$

here, χ'' is the imaginary part of magnetic susceptibility, $\eta = \int_s h^2 dV/\int_r h^2 dV$ is the filling factor, h is the microwave magnetic field, the first and second integrals are taken over the sample volume and over the resonator volume, respectively, $Q = f_{\rm res}/(2\delta_{1/2})$ is the quality factor of the empty loaded resonator, $\delta_{1/2}$ is the half width at half maximum of the resonance curve, and U_0 is the signal passing through the resonator in the absence of the sample. The typical values of Q for the resonators are 3000–5000.

The change $\delta\chi'$ in the real part of the susceptibility with the magnetic field may be derived from measurements of $f_{\rm res}$ using the following relation [20]:

$$\delta f_{\rm res} = -4\pi\gamma\eta\,\delta\chi' f_0, \tag{3}$$

here, $\delta f_{\rm res}$ is the field-induced shift of the $f_{\rm res}$, f_0 is $f_{\rm res}$ at the zero field, and γ is a numerical coefficient which depends on the shape of the sample (for a spherical sample, it equals 1). Using these principles, we estimated the real and imaginary parts of the magnetic susceptibility of the sample from measurements of the resonance curve of the resonator. Factor γ was taken to be 1, and the typical value of the filling factor was 0.01 for the cylindrical resonator and 0.005 for the rectangular one.

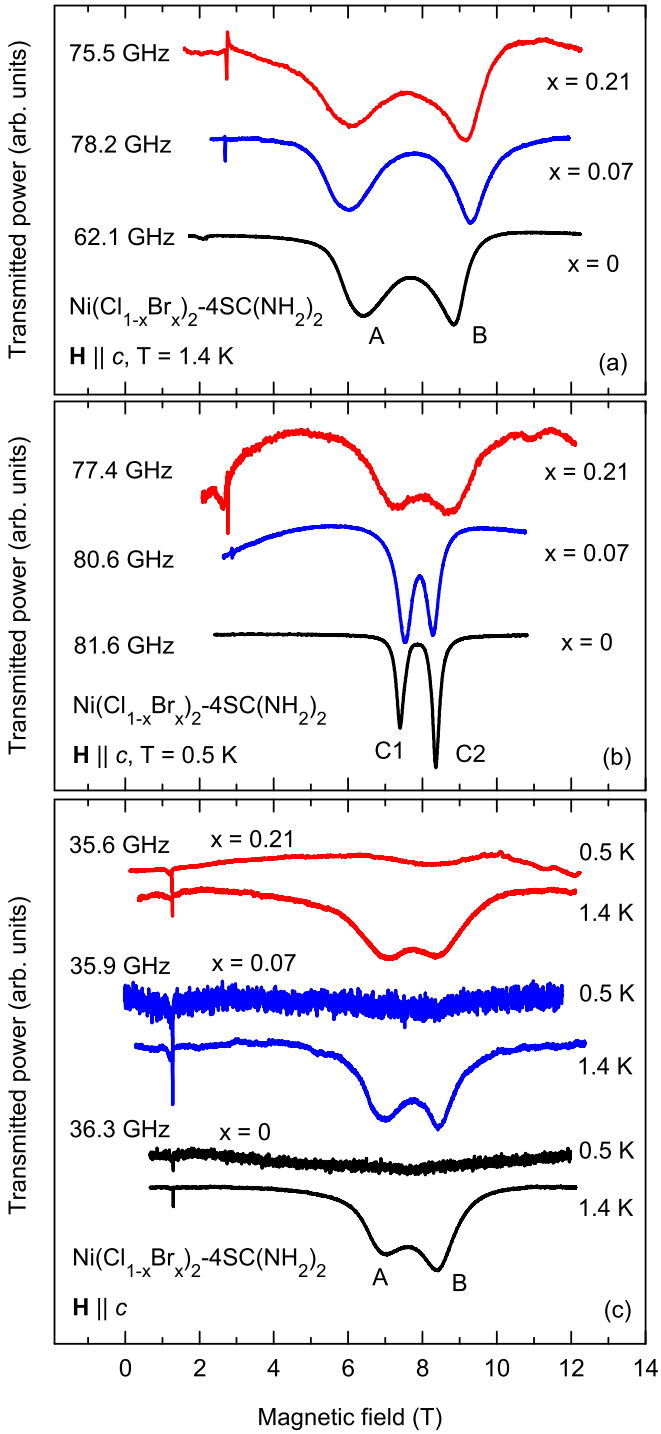

FIG. 1. Examples of ESR lines obtained in DTNX with $x = 0, 0.07, 0.21$ for $\mathbf{H} \parallel c$. Panel (a) ESR lines in the paramagnetic phase, panel (b) ESR lines in the ordered phase at $T = 0.5$ K, and (c) ESR records for $T = 1.4$ and $T = 0.5$ K at $f < \Delta_2$.

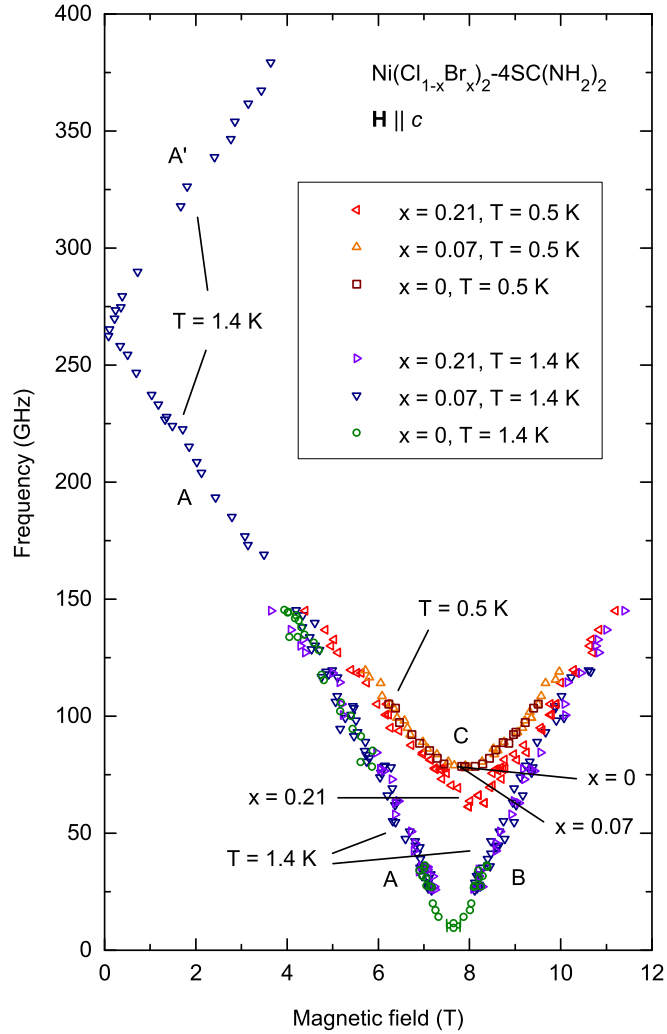

FIG. 2. The frequency-field dependences of ESR in DTN and DTNX measured at $T = 0.5$ and $T = 1.4$ K for $\mathbf{H} \parallel c$.

IV. EXPERIMENTAL RESULTS

A. ESR spectra at H ∥ *c*

The three upper curves in Fig. 1 are taken at $T = 1.4$ K and demonstrate examples of ESR absorption in the paramagnetic phase for samples with different Br concentrations. The resonance fields presented in the frequency-field diagram (Fig. 2) demonstrate that, in the paramagnetic state, the frequency-field dependence is the same for all Br concentrations. The observed paramagnetic spectrum has a nonzero frequency Δ_1 in the zero field, this mode is split by a magnetic field into two branches, descending (A) and ascending (A'). The descending branch falls almost to zero and is replaced by a new ascending branch B. This spectrum is similar to that of spin $S = 1$ in an axial crystal field [21]. For a spin in a crystal field, the $f(H)$ dependencies of modes A, A', and B are linear. For DTN, there is a weak deviation from linear dependence. The zero-field frequency we observe for the $x = 0.07$ sample is 265 ± 3 GHz. This coincides well with a value of 270 ± 5 GHz measured in ESR experiments of Ref. [15] and a gap of 1.06 ± 0.04 meV (256 ± 10 GHz) measured in neutron experiments with pure samples [9]. The value of Δ_1 for $x = 0.21$, measured in neutron-scattering experiments 1.1 meV [13,14] is almost the same. We observe that branches A and B in the paramagnetic phase (at $T = 1.4$ K) cross at a frequency of 10 GHz.

The temperature evolution of ESR lines is presented in Figs. 3 and 4. Upon cooling below 1.2 K, we observe a gradual convergence of resonance modes A and B. At the

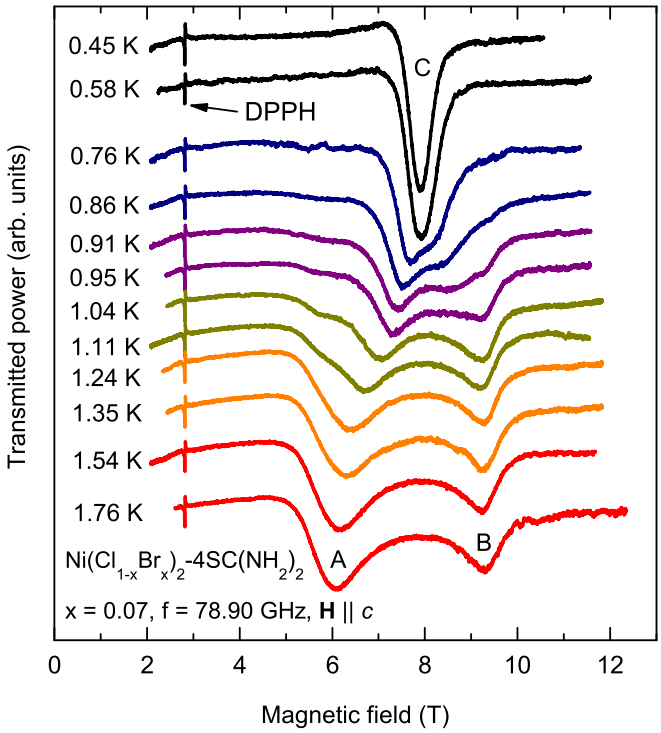

FIG. 3. Temperature evolution of ESR spectra taken at $f = 78.90$ GHz and $\mathbf{H} \parallel c$ in DTNX with $x = 0.07$.

low-temperature of $T = 0.5$ K, the two lines are closer than in the paramagnetic phase as presented in Figs. 1, 3, and 4. Near the middle of the field interval of the antiferromagnetic phase, lines A and B merge, forming a mode C. Mode C has

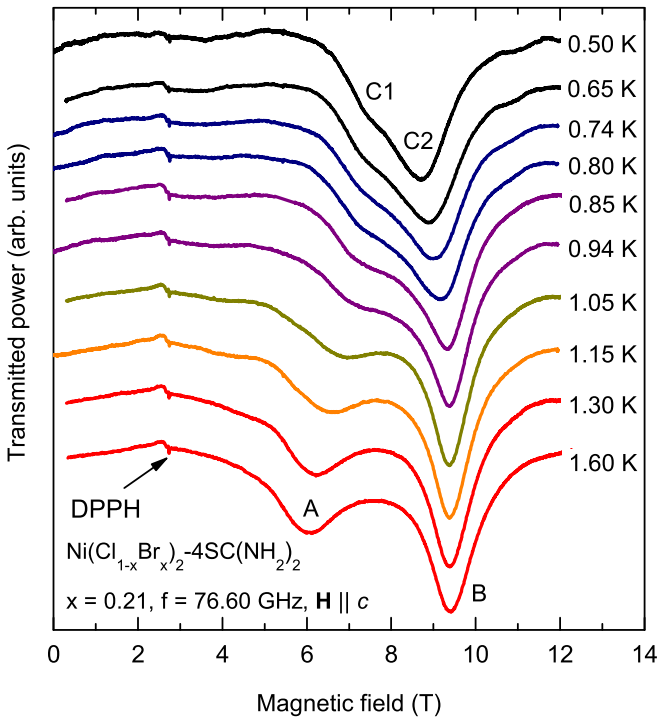

FIG. 4. Temperature evolution of ESR spectra taken at $f = 76.60$ GHz and $\mathbf{H} \parallel c$ in DTNX with $x = 0.21$.

a minimum frequency Δ_2, which may be considered as an AFMR gap. For $x = 0$ and $x = 0.07$ samples, the AFMR gap in the low-temperature limit is 78 GHz. The substitution of Cl with Br results in a broadening of the AFMR line and a change in the temperature-induced shift of resonance lines. In a sample with $x = 0.21$, the temperature-dependent shift of lines A and B is smaller than in the $x = 0$ and $x = 0.07$ samples, the gap Δ_2 is also smaller and equals 65 GHz instead of 78 GHz in a pure sample, see Fig. 2. Figure 4 demonstrates that, for a sample with a large Br concentration, 76-GHz ESR is a doublet, corresponding to the overgap range. At the same time, the $x = 0.07$ sample has a single ESR line indicating a gap frequency at 78 GHz, see Fig. 3. This clearly proves a larger value of the gap for the $x = 0.07$ and $x = 0$ samples. In addition, the minimum position for the gapped mode C shifts towards higher fields in the $x = 0.21$ sample for about 0.2 T. In the subgap frequency range (below Δ_2), the ESR signal completely disappears at cooling, see the 36-GHz ESR lines in Fig. 1.

B. ESR in a tilted field

In the ordered phase, at a precise orientation of the magnetic field along the c axis, we do not observe any resonances at the frequencies below gap Δ_2. Upon tilting the magnetic field with respect to the c axis, a pair of ESR lines appears. Their frequency increases with tilting. ESR lines taken at different field angles relative to the c axis and the corresponding frequency-field dependencies are shown in Fig. 5. The larger the deviation of the field from the c axis on the ac plane, the greater the frequency of these modes (they are marked as modes $D1, D2$). At changing the magnetic field, the frequency of the $D1, D2$ modes approaches zero at both boundary fields H_{c1}, H_{c2} and reaches a maximum value in the middle of the field range of the ordered phase, i.e., near 8 T. We assume that these resonances have zero frequency at the exact orientation $\boldsymbol{H} \parallel c$. We estimate the accuracy of the sample orientation in our experiments as about 1°. This may be due to the disorientation of the resonator with respect to the solenoid.

The temperature evolution of the pair of ESR lines in a magnetic field tilted by 6° away from the c axis is shown in Fig. 6. It demonstrates that the D resonances exist only at low temperatures in the ordered phase.

C. Dynamic diamagnetism in the ordered phase

At cooling the samples below the Néel temperature, we detect a significant change δf_{res} in the resonance frequency of the resonator in a range where ESR absorption is not observable. This low-temperature frequency shift appears only in the field range of the ordered phase, i.e., between fields H_{c1} and H_{c2}. We have measured δf_{res} in different fields and for different resonance modes of different resonators and found that the corresponding change in the real part of the dynamic magnetic susceptibility χ' appeared to be negative (i.e., diamagnetic) and exists above the low-frequency mode D.

To characterize this observation quantitatively, we recorded resonance curves of the resonator in a field range from zero to 12 T with a step of about 0.05 T. The analysis of resonance

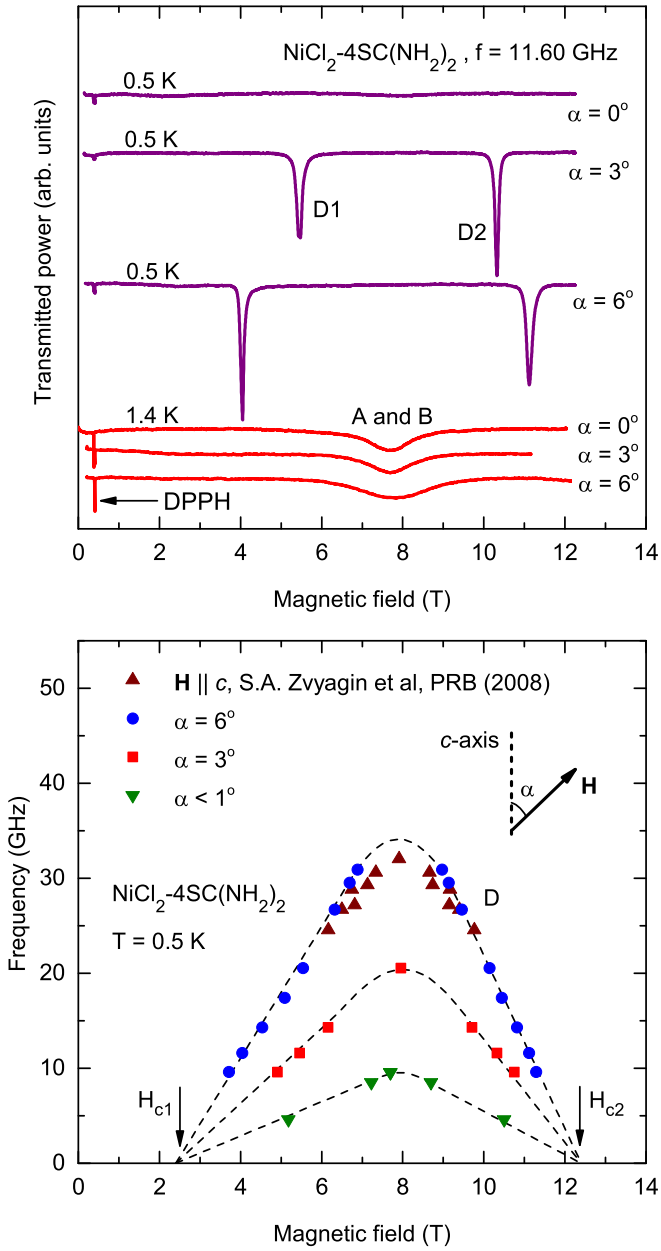

FIG. 5. The 11.6-GHz ESR absorption curves at 0.5 and 1.4 K (upper panel) and the frequency-field diagrams for ESR in a low-frequency range at 0.5 K (bottom panel) obtained in pure DTN for different orientations of the magnetic field in relation to the c axis.

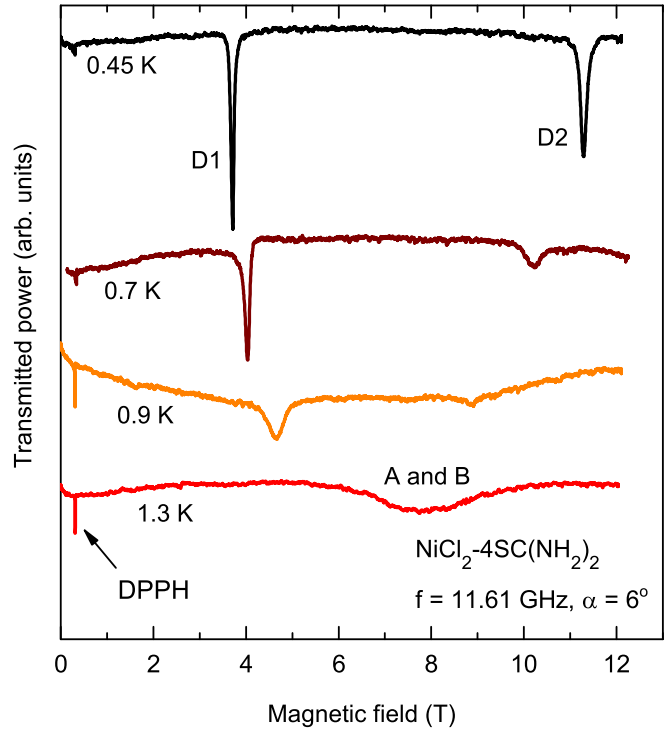

FIG. 6. Temperature evolution of the ESR line taken in pure DTN at a frequency of $f = 11.6$ GHz for the magnetic field tilted by 6° from the c axis.

curves gives dependencies of resonator frequency, amplitude, and width on the magnetic field. From these values, we deduce changes in susceptibilities χ' and χ''. The capability of this method for the DTN samples was tested in the paramagnetic phase at $\boldsymbol{H} \parallel c$ and $T = 1.4$ K for the 31.70-GHz TM_{211} mode of the cylindrical resonator of a diameter 16 mm. The results are presented in Fig. 7.

In the upper panel, we see that the transmitted signal and the amplitude of the resonator resonance curve demonstrate the identical field dependencies. The frequency shift of the resonator is presented in the lower panel. This curve may be well fitted by two dispersion curves of two Lorentzian resonances corresponding to modes A and B. The dispersion curves are known to represent the susceptibility χ' for a standard Lorentzian ESR curve. These dispersion curves, presented by dashed lines, are of inverted types because the A frequency is falling whereas the B frequency is rising with the magnetic field. The field dependence of the amplitude of the resonator curve may be well reconstructed by two Lorentzian curves with the same resonance fields and widths as for dispersion curves. This reconstruction is presented by a dotted line in the upper panel of Fig. 7. Thus, the observed response of the resonator to changes in χ' and χ'' of the sample corresponds well to the known changes of susceptibilities near paramagnetic resonance fields.

The resonator curves for the ordered phase are presented in panel (a) of Fig. 8. These data are taken in different fields $\boldsymbol{H} \parallel c$ and $T = 0.5$ K for the 27.05-GHz TE_{112} mode of the same cylindrical resonator. One can see that, at low temperatures, the increase in magnetic field causes a shift of the resonance curve towards higher frequencies. This shift has a maximum at $H = 8$ T and then comes back to zero at $H = 12$ T. By a Lorentzian fit to these curves, we obtained the field dependence of $\delta f_{\rm res}$. The positive value of $\delta f_{\rm res}$ indicates a significant negative change in χ' in the field interval between the critical fields H_{c1} and H_{c2}. We estimated $\delta\chi'$ using Eq. (3), the maximum absolute value is about 0.2 emu/mol. From the comparison of the low-temperature $\delta f_{\rm res}(H)$ curve [upper line in Fig. 8(b)] and of the $\delta f_{\rm res}$ curve of the paramagnetic phase (lower line), we conclude that the nonresonant low-temperature susceptibility χ' has approximately the same value as one at paramagnetic resonance. Furthermore, because χ' of the paramagnetic resonance exceeds the static susceptibility for a Q factor of the paramagnetic resonance

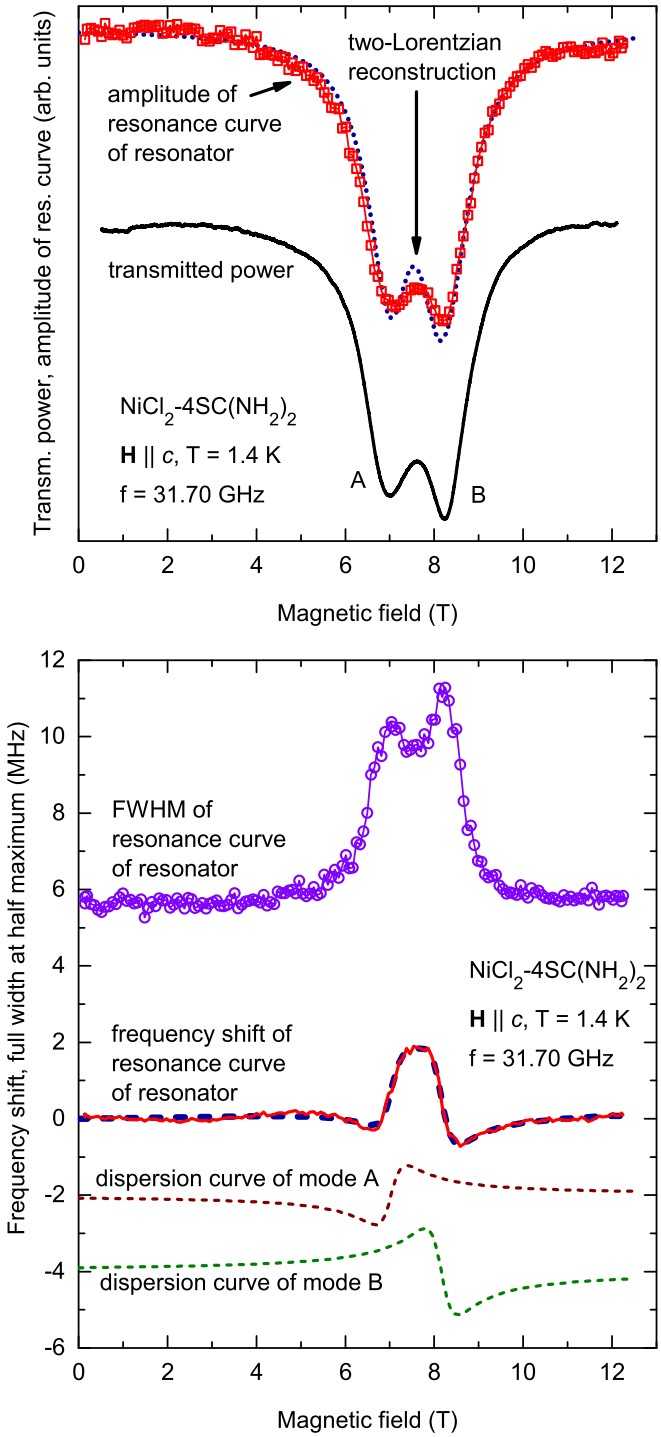

FIG. 7. Upper panel: amplitude of resonator curve vs magnetic field for 31.70 GHz (symbols) and ESR record at $T = 1.4$ K (solid line). The dotted line is the two-Lorentzian model modified for high sample volume. Resonance fields and full width at half maximum (FWHM) for Lorentzians are the same as for dispersion curves on the lower panel. Bottom panel: Frequency shift and FWHM of the resonator vs field. The dashed line imposed on the frequency shift curve is a fit by two dispersion curves (dashed lines) for Lorentzian resonances.

[22] (here, $Q \simeq 2$) and considering the sum of contributions of two close lines A and B, we conclude that $\chi' \simeq 4\chi_0 \simeq$ 0.4 emu/mol. Here, $\chi_0 = 0.1$ emu/mol is the value of the order of low-temperature differential static susceptibility [5]. This is in reasonable correspondence with the above estimate from the absolute value of $\delta f_{\rm res}$.

The amplitude of the resonance curve of the resonator demonstrates a reduction in the ordered phase, see Fig. 9(b). This indicates the increase in χ'' of about 20% of the maximum value of $|\chi'|$. The dependence of the frequency shift of the resonator on the magnetic field at $T = 0.5$ K clearly shows that the shift appears between 2.5 and 12 T, marking the critical fields of the ordered phase at 0.5 K. The temperature evolution of the dependencies of resonance frequency on the magnetic field shown in panel (b) of Fig. 8 demonstrates the decrease in $\delta f_{\rm res}$ and $|\chi'|$ at the temperature rise. At temperatures $T > 1$ K, the frequency shift $\delta f_{\rm res}$ is observable only near the resonance fields of modes A and B of the paramagnetic phase. A similar temperature evolution of the frequency shift dependence on the magnetic field was measured in DTNX with $x = 0.21$ at $\boldsymbol{H} \parallel c$ for the 35.29-GHz TE_{012} mode [see panel (c) of Fig. 8]. These data additionally prove the coupling of dynamic diamagnetism to the order parameter. They illustrate that, at 0.5 K, the peak position of the resonance curve starts to deviate exactly at the zero field. This confirms the formation of the ordered state in the zero field as manifested in Ref. [13]. We detected dynamic susceptibility at frequencies up to the upper AFMR branch C. An example of $\delta f_{\rm res}$ records for the highest frequency of detailed measurements 62.05 GHz is given in Fig. 9 panel (c). Because of the uncertainty in the filling factor for different modes of the resonator when the electromagnetic wavelength is comparable to the size of the sample, we are unable to derive the exact numerical value of χ' and its frequency dependence. Nevertheless, we claim it is always negative within the antiferromagnetic phase, and it is comparable with the dynamic susceptibility of the paramagnetic resonance at $T = 1.4$ K within the range of 9–75 GHz. The measurement of the dynamic susceptibility at higher frequencies is prevented by a strong ESR response of branch C as well as by the close mutual proximity of the modes of the resonator, which results in their overlapping. For the frequencies of 99 and 119 GHz, we observe characteristic kinks in the transmitted power records at fields of 2.5 and 12 T which indicate the start and finish of the nonresonant response still present at these frequencies.

To test the bottom of the frequency range of the dynamic diamagnetic susceptibility, we have measured $\delta f_{\rm res}$ at low frequencies using a rectangle resonator of the size $40 \times 8 \times 17$ mm with TE_{013}, TE_{012}, and TE_{011} modes for the field tilted from the c axis. As an example, the experimental results for measurements at the frequency of 11.6 GHz with mode TE_{012} are presented in the upper panel of Fig. 10. For intermediate fields strictly between resonance positions of two type-D modes, we observed the suppression of the effect of dynamic diamagnetism. Thus, when the frequency is lower than the frequency of the lower AFMR mode D, the diamagnetic contribution to the dynamic susceptibility practically disappears. From this observation at all three frequencies, we deduce that the negative χ' at low temperatures exists at frequencies down to that of the quasi-Goldstone mode where it abruptly vanishes.

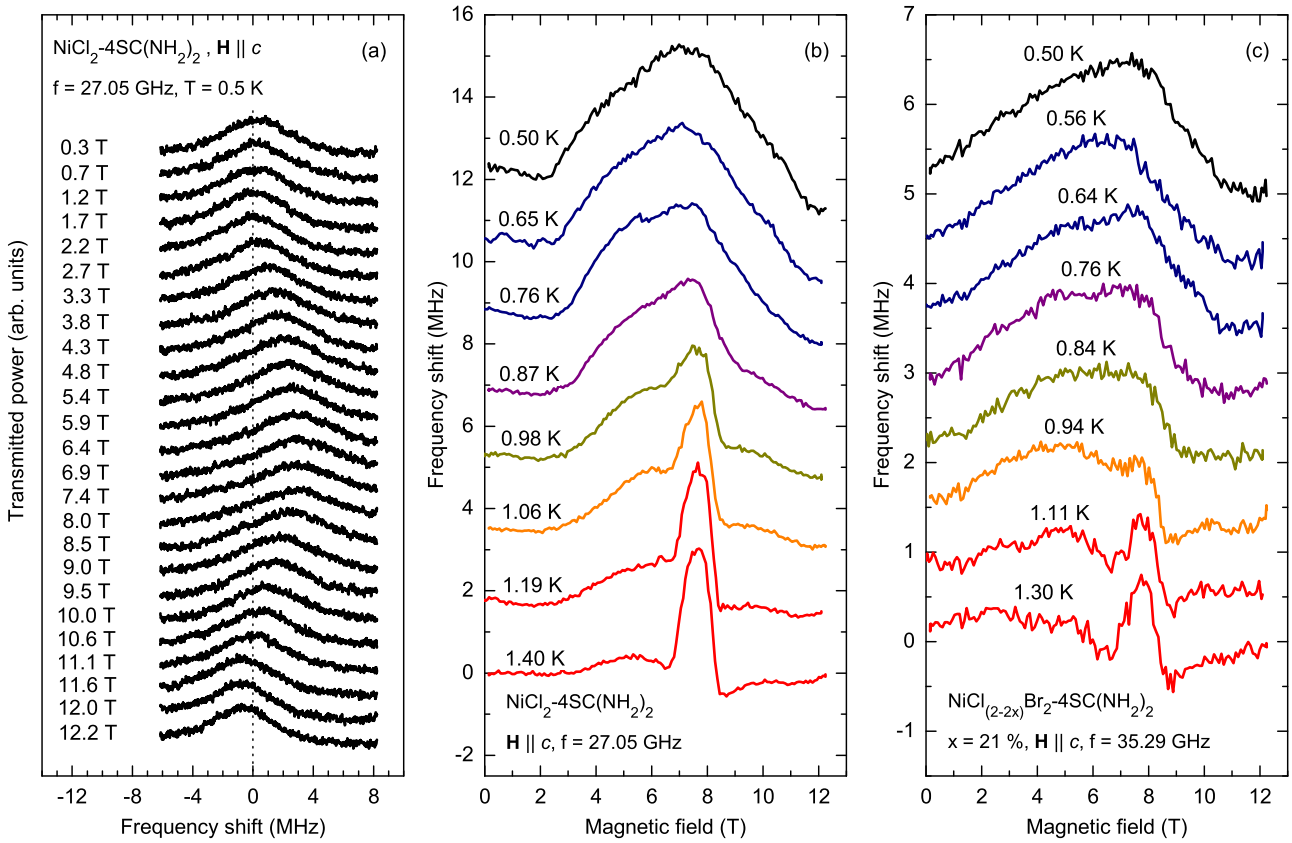

FIG. 8. Panel (a) examples of resonance curves of resonator with a DTN sample for the 27.05-GHz TE_{112} mode at 0.5 K and different values of field $\mathbf{H} \parallel c$. Panel (b) temperature evolution of dependencies of resonance frequency shift on magnetic-field $\mathbf{H} \parallel c$, $f = 27.05$ GHz. The lines are shifted vertically by 1.75 MHz from each other. Panel (c) temperature evolution of $\delta f_{\rm res}$ for the 35.29-GHz (TM_{021}) mode of the resonator with DTNX sample $x = 0.21$. The lines are shifted vertically by 0.75 MHz from each other.

We ascribe the observed nonresonant susceptibilities χ' and χ'' to dynamic magnetization on the (ab) plane because of the standard ESR configuration of microwave fields used where the rf magnetic field is perpendicular to the static field. We measured also the frequency shift of the resonator placing the sample at the maximum of the microwave electric field, which is perpendicular to the external field. Then, the sample was positioned at the maximum of the longitudinal microwave field. In both cases, the shift was not greater than that for the initial sample position at the maximum of the transverse microwave field. At the same time, the intensity of the paramagnetic ESR was reduced only by a factor of 2 in comparison with the initial experiment. This indicates a presence of all components of the microwave fields in the sample, i.e., we have a mix of polarizations of microwave fields within the sample, and a quantitative polarization experiment is impossible because of a large size of the sample. The sample of a size of 3 to 4 mm is comparable to a quarter of the electromagnetic wavelength in the dielectric sample with $\varepsilon \simeq 4$. However, the fraction of the sample volume with a certain polarization of electric or magnetic microwave field was changed, and no sufficient increase in the diamagnetic response was observed. This means that the observed nonresonant dynamic susceptibility is mainly due to the transverse magnetization oscillation.

V. DISCUSSION

A. Paramagnetic resonance and AFMR gap

The paramagnetic resonance at $T = 1.4$ K is mainly analogous to the ESR spectrum of a spin $S = 1$ in a crystal field. It has a gap in the zero field and a descending branch which reaches approximately zero frequency for a precise orientation of the magnetic field along the fourfold axis. We observe the zero-field gap $\Delta_1 = 270$ GHz and a decreasing branch with the minimum frequency of 10 GHz. This nonzero frequency could be ascribed to the misorientation of about 1°, our accuracy of the orientation of the sample. Naturally, this lower frequency might be also affected by other weak interactions.

For the ordered phase, we observe a broadening of resonance lines under Br substitution of DTN which is naturally due to random variation of local surrounding of magnetic ions (see Fig. 1). The most significant modification of the ESR spectrum caused by Br impurities is a decrease of the AFMR gap Δ_2.

In the molecular field theory of Ref. [15], the value of Δ_2 is approximately proportional to J, and the field of the minimum of the frequency of mode C rises approximately linear in D. The calculation by the method described in Ref. [15] results in the following approximate dependence of Δ_2 and of the field

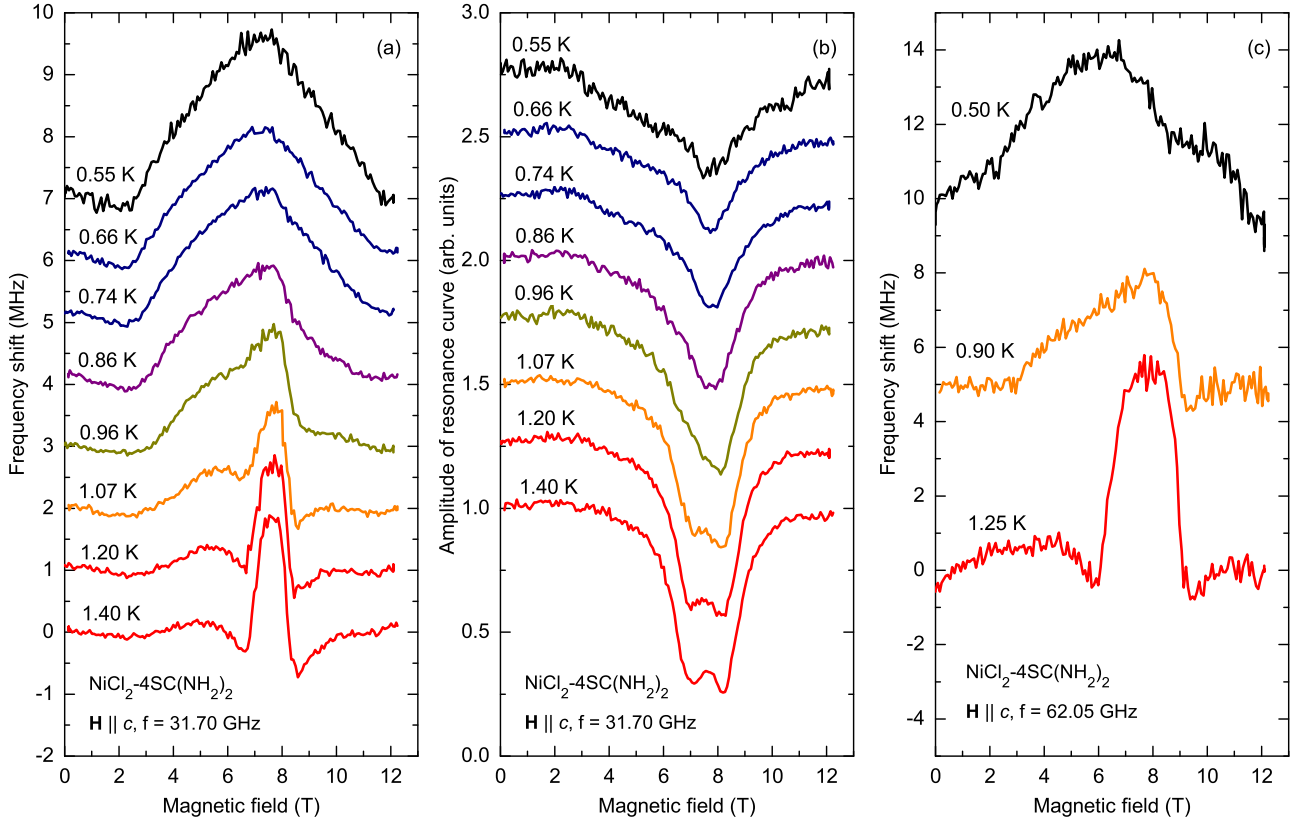

FIG. 9. Panel (a) temperature evolution of the field dependence of the frequency shift $\delta f_{\rm res}$ on magnetic-field $\mathbf{H} \parallel c$ for the 31.70-GHz TM_{211} mode. The lines are vertically shifted, in turn, by 1 MHz. Panel (b) temperature evolution of the field dependence of the amplitude of the 31.7-GHz mode. The lines are normalized to the zero-field amplitude for each of the temperature values and vertically shifted, in turn, by 0.25 a.u. Panel (c) frequency shift for the 62.05-GHz mode of the resonator. The lines are vertically shifted, in turn, by 5 MHz.

of the minimum of AFMR frequency $H_{\rm res}$ on J and D:

$$\frac{\partial \Delta_2}{\partial J} = 45.7\ \text{GHz/K}, \quad \frac{\partial \Delta_2}{\partial D} = -0.6\ \text{GHz/K},$$
$$\frac{\mu_0 \partial H_{\rm res}}{\partial J} = 0.69\ \text{T/K}, \quad \frac{\mu_0 \partial H_{\rm res}}{\partial D} = 0.66\ \text{T/K}.$$

These differential relations are valid in the vicinity of the experimental values of $\Delta_2 = 78$ GHz, $H_{\rm res} = 8$ T. From the observed decrease in Δ_2 for 13 GHz and an increase in $H_{\rm res}$ for 0.2 T, we get the change in the exchange integral $\delta J = -0.3$ K and the change in anisotropy parameter of $\delta D = 0.7$ K. These values contradict substitution-induced changes in parameters J and D derived in Ref. [14]. Here, the zero-field dispersion curves of excitations in DTNX were interpreted within a so-called generalized spin-wave theory [23,24]. This analysis of $x = 0.21$ data resulted in the opposite and much stronger changes: $\delta J = 0.75$ and $\delta D = -1.5$ K with respect to the parameters of a pure compound reported in Ref. [6].

Recently another approach for the calculation of the AFMR spectrum in the field-induced antiferromagnetically ordered phase was suggested, which implies a $1/S$ expansion for the order parameter and resonance frequencies [25]. Here, a significant influence of the interchain exchange is predicted whereas the effects of parameters J and D on gap Δ_2 and $H_{\rm res}$ are of the same sign as in the theory of Ref. [15]. In this approach, for DTN, we have

$$\frac{\partial \Delta_2}{\partial J} = 125\ \text{GHz/K}, \quad \frac{\partial \Delta_2}{\partial D} = -40\ \text{GHz/K},$$
$$\frac{\mu_0 \partial H_{\rm res}}{\partial J} = 0.67\ \text{T/K}, \quad \frac{\mu_0 \partial H_{\rm res}}{\partial D} = 0.33\ \text{T/K}.$$

This corresponds to changes $\delta J = -0.1$ and $\delta D = 0.6$ K and is in a contradiction with the above interpretation of zero-field neutron scattering.

The above simple interpretation of the antiferromagnetic resonance in the Br-substituted samples appears to be controversial also because the effective parameters of exchange and anisotropy, deduced from the observed AFMR frequency and field correspond to a disordered phase in the Sakai-Takahasi phase diagram [2,4] (indeed, $D/J > 5$ at $J_{ab}/J = 0.08$) correspond to a quantum paramagnet instead of the observed antiferromagnetic phase of this sample of DTNX. Both these contradictions indicate that AFMR in Br-substituted samples cannot be described in the same way as in the pure sample with just renormalized parameters of J and D. The approach to a strongly inhomogeneous system of DTNX as to a homogeneous one with renormalized parameters may be wrong because the local variation of exchange and anisotropy at a Br-substituted site is more than 100% as suggested by the NMR study [16]. Local parameters for a magnetic ion near impurity are substantially affected, and the influence of

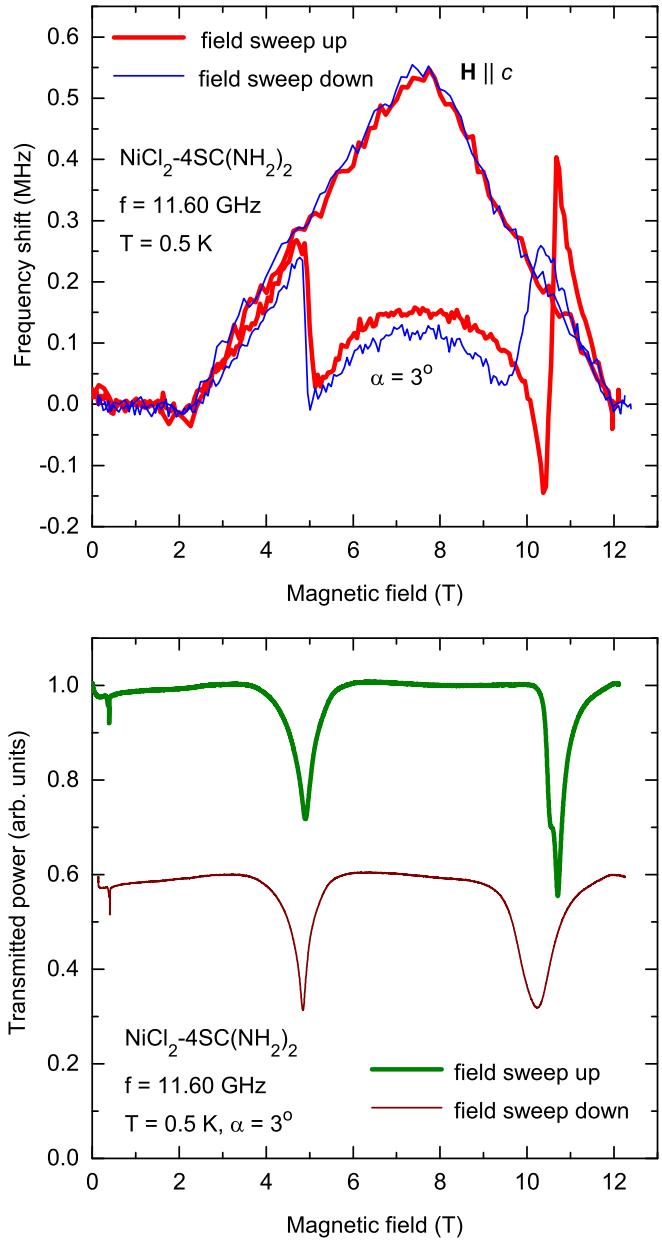

FIG. 10. Dependencies of resonance frequency shift on the magnetic field for the 11.6-GHz mode of the resonator (upper panel) and the ESR absorption lines (bottom panel) measured at $T = 0.5$ K for $\mathbf{H} \parallel c$ and for the field tilted by 3° from the c axis. ESR lines are normalized to 1, and the lower line is shifted down by 0.4.

impurities may be more complicated than their renormalization. An example of a cardinal change in the effective Hamiltonian by a nonmagnetic substitution was given in Refs. [26,27]. An additional interaction in the form of a biquadratic exchange was shown to appear in a frustrated system with a chaotic modulation of the exchange network. In this case, the effective Hamiltonian of the crystal with impurities should be corrected for additional terms.

B. Quasi-Goldstone AFMR in a tilted field

Low-frequency resonances observed in DTN in a tilted field clearly originate from a zero-frequency Goldstone mode, which should exist at the exact orientation of the magnetic field along the c axis [15]. At a tilting of the magnetic field, the axial symmetry is lost, and the degeneracy of spin configurations with respect to rotation around the c axis is lifted. This should result in a nonzero frequency of spin oscillations. Indeed, as may be seen in Fig. 5 with increasing the deviation angle, the resonance frequency increases. The frequency of this oscillations drops to zero at the boundary fields of the antiferromagnetic phase. This is natural since the order parameter also vanishes at these fields. In contrast to the earlier conclusion of Ref. [15], we now believe that the low-frequency resonance branch D appears due to the tilting of the magnetic field and that is not an exchange branch of two interpenetrating antiferromagnetic systems. The frequency of the exchange mode in the case of frustration is an intriguing and challenging problem. From a qualitative point of view, the frequency of the exchange mode is probably much lower since the corresponding exchange integral J'' is rather weak. Its value of 0.08 K corresponds to 1.6 GHz. Moreover, this interaction is frustrated as the molecular fields of the corner-site spins cancel each other at the center-cell site. The expected exchange branch should have a frequency far below 1.6 GHz, which is out of our frequency range and may be masked by weak interactions.

C. Dynamic diamagnetism in the ordered phase

The nature of the observed dynamic diamagnetism of the ordered phase of DTN is not clear at the present moment. A simple example of dynamic diamagnetism is given by a conventional ESR in a paramagnet where a negative χ' exists in a narrow range above the ESR frequency, see, e.g., Ref. [22]. This kind of diamagnetism should exist only near the resonance frequency and disappear below the frequency of ESR. In our experiments, we observe a strong diamagnetic response in a wide frequency range. This range has a sharp lower boundary at the frequency of mode D. In the upper direction, it spreads, at least, to the frequency of about 100 GHz. The frequency-field range of the nonresonant dynamic susceptibility is schematically shown in Fig. 11. To explain the observation of the intensive dynamic diamagnetic susceptibility in a wide frequency range, we propose this is due to a coupling of microwave field to magnon pairs. Two kinds of this coupling were suggested, see, e.g., Refs. [20,28]. For the coupling of the first type, the power of the microwave pumping of the frequency f is absorbed by pairs of magnons with a half frequency $f/2$ and opposite wave-vectors $\boldsymbol{k}$. This coupling results in the parametric excitation of magnons when the microwave field exceeds a threshold value. The parametric excitation is also known as Suhl's instability of the first kind. The parametric resonance condition $f = f(\boldsymbol{k}) + f(-\boldsymbol{k}) = 2f(\boldsymbol{k})$ is necessary for this coupling. Above the threshold, the magnon number rises exponentially in time, and finally it is limited by an additional nonlinearity at a higher level. Below the threshold, in a stationary regime, thermally activated pairs of magnons absorb the power from the pumping which results in the subthreshold absorption. This effect corresponds to a microwave susceptibility in a wide range between the doubled minimum and the doubled maximum frequencies of the magnon branch. The theory of subthreshold absorption was

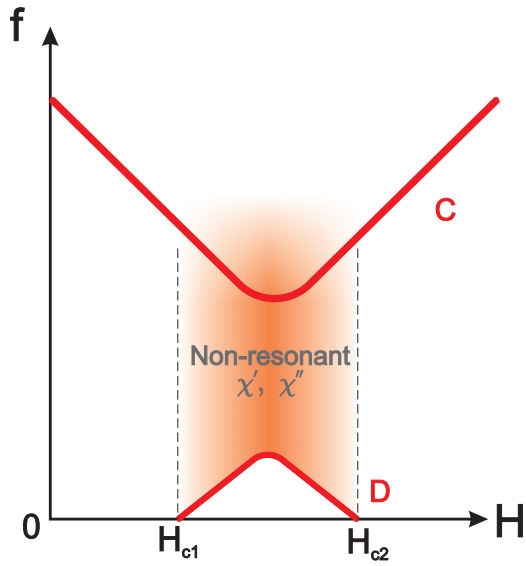

FIG. 11. Scheme of the frequency-field range of the nonresonant dynamic response of DTN.

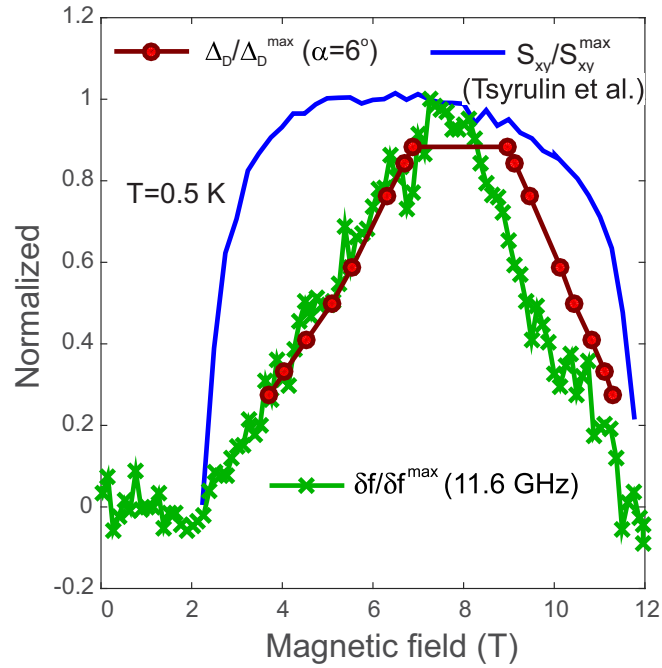

FIG. 12. Comparison of the field dependencies of the order parameter measured in the neutron-scattering experiments of Ref. [6] with the observed values of the resonator frequency shift and of the frequency of the quasi-Goldstone mode in a tilted field.

suggested in Ref. [29], experimental observations are reported in, e.g., Refs. [30–32].

Another coupling of a microwave magnetic field and pairs of magnons is the reason for Suhl's instability of the second kind. It results in the saturation of ferromagnetic resonance. Two quanta of microwave pumping are converted into two magnons with opposite wave-vectors $\boldsymbol{k}$ and $-\boldsymbol{k}$ corresponding to a resonance condition $2f = 2f(\boldsymbol{k})$. This coupling [28] originates from a nonlinear interaction of the uniform spin precession excited by the microwave field with the spin-wave modes with wave-vectors $\boldsymbol{k}$, $-\boldsymbol{k}$. The frequency range for the microwave absorption due to this mechanism is strictly between the bottom and the top of the spin-wave branch. The subthreshold absorption due to coupling of Suhl's second kind is, in principle, possible, but not confirmed in experiments.

For DTN, we may suppose the upper AFMR branch C as a source of the uniform spin oscillations, which are excited at a lower wing of its resonance curve (it has a linewidth of about 15 GHz). Then, pairs of magnons of the D branch may be excited by the coupling of the second kind. The magnons of the D branch have a dispersion range which may be estimated as $2J_c\sqrt{S(S+1)} \simeq 110$ GHz. This estimate is in correspondence with the observed [6] dispersion range of 0.4 meV = 97 GHz of the lower magnon branch in a magnetic field of 6 T. The range of two-magnon absorption with the coupling of the second kind corresponds well with the range of the nonresonant susceptibility observed in DTN. We identify the lower-frequency limit exactly on the AFMR frequency of the D mode and see that the whole range propagates above 100 GHz. At a frequency below the uniform precession of mode D, this coupling should be terminated as we observe in the experiment with the tilted field when the dynamic diamagnetism drops at a field of D-type resonance.

The subthreshold absorption observed in Refs. [30–32] was recorded as an imaginary part of the dynamic susceptibility. The peculiar features of wide-range dynamic susceptibility of DTN are that the coupling is of the Suhl's second kind, diamagnetic susceptibility χ' dominates over the imaginary part χ'', and the low-frequency cutoff of the effect corresponds to the resonance frequency of the uniform mode and not to the doubled frequency of this mode. The imaginary part of the dynamic susceptibility should be inevitably accompanied by the real part according to Kramers-Kronig relations. This justifies the real part of the dynamic susceptibility. The dynamic susceptibility for the parametric excitation (Suhl's instability of the first kind) of spin waves in an antiferromagnet was also found to have a significant diamagnetic real part [33].

It is worth noting that the diamagnetic susceptibility and the frequency of the quasi-Goldstone mode in a tilted field have practically coinciding field dependencies. Both χ' and f_D have zero values at the boundaries of the antiferromagnetic phase and demonstrate a maximum in a form of an apex of a triangle. The order parameter also is zero at the critical fields $H_{c1,2}$. However, it has a wide maximum in the middle of the range. The comparison of the field dependencies of these three parameters is shown in Fig. 12.

Summarizing the discussion of the dynamic diamagnetism of DTN, we conclude that we have only a quite hypothetical explanation for this effect. We explain a wide-range dynamic susceptibility via the coupling between the microwave pumping and the pairs of magnons. This coupling is probably of the same type as for the Suhl's instability of the second type. In principle, other mechanisms of transformation of the uniform spin oscillation mode to spin waves, e.g., by elastic scattering by defects might also result in a wide range of dynamic response with observed boundaries.

D. Unsolved problems

We note the following questions which are not yet discussed in theory, that would be of importance for understanding of peculiar properties of DTN. First, this is the theory of the spin dynamics and AFMR of the quantum magnet beyond the critical field of the field-induced ordering, including the field range where the order parameter is weak. The second unsolved problem is the theory of spin oscillations of an antiferromagnet with a body-centered lattice with two interpenetrating antiferromagnetic subsystems, the exchange interaction of which is frustrated in a molecular field approximation. It should, probably, contain a consideration of order-by-disorder mechanism for derivation of the ground state. The third question is the physical nature of a continuum of spin modes providing a wide range of dynamic diamagnetism.

VI. CONCLUSIONS

We have observed experimentally the following new features of the spin dynamics of chain $S = 1$ anisotropic antiferromagnet $NiCl_2$-4SC$(NH_2)_2$.

(1) The spectrum of antiferromagnetic resonance consists of two branches, one of them is gapped and has the minimum frequency of 78 GHz in the low-temperature limit, and the other is the zero-frequency Goldstone mode.

(2) The Goldstone mode acquires a gap at a small tilting of the field with respect to the fourfold axis of the crystal.

(3) At a nonmagnetic substitution, replacing 21% of Cl ions by Br ions, the gap of the upper AFMR branch is reduced.

(4) There is a wide range of the strong dynamic diamagnetic response at the frequencies above the quasi-Goldstone mode. This dynamic diamagnetism is proposed to appear due to a wide-range coupling of two-magnon states of a quasi-Goldstone mode D to a microwave magnetic field.

ACKNOWLEDGMENTS

We are indebted to A. K. Kolezhuk, A. V. Syromyatnikov, and O. I. Utesov for valuable discussions and performing theoretical calculations of AFMR frequencies and giving us the results of their calculations before publication, S. A. Zvyagin for valuable comments, M. E. Zhitomirsky, L. E. Svistov, S. S. Sosin, and V. N. Glazkov for numerous important discussions. The work at the Kapitza Institute (ESR experiments, microwave measurements, and data processing) was supported by the Russian Science Foundation, Grant No. 17-12-01505. Construction and installation of the 4.5-GHz spectrometric unit was supported by the Russian Foundation for fundamental research (Grant No. 19-02-00194). Analysis of two-magnon absorption was supported by the Program of Presidium of RAS. The sample preparation work performed at the University of São Paulo was supported by the Brazilian Agency FAPESP (Grant No. 2015-16191-5).

[1] F. D. M. Haldane, Continuum dynamics of the 1-D Heisenberg antiferromagnet: Identification with the O(3) nonlinear sigma model, Phys. Lett. A **93**, 464 (1983).

[2] T. Sakai and M. Takahashi, Effect of the Haldane gap on quasi-one-dimensional systems, Phys. Rev. B **42**, 4537 (1990).

[3] K. Wierschem and P. Sengupta, Quenching the Haldane Gap in Spin-1 Heisenberg Antiferromagnets, Phys. Rev. Lett. **112**, 247203 (2014).

[4] K. Wierschem and P. Sengupta, Characterizing the Haldane phase in quasi-one-dimensional spin-1 Heisenberg antiferromagnets, Mod. Phys. Lett. B **28**, 1430017 (2014).

[5] A. Paduan-Filho, X. Gratens, and N. F. Oliveira, Field-induced magnetic ordering in $NiCl_2 \cdot 4SC(NH_2)_2$, Phys. Rev. B **69**, 020405 (2004).

[6] N. Tsyrulin, C. D. Batista, V. S. Zapf, M. Jaime, B. R. Hansen, C. Niedermayer, K. C. Rule, K. Habicht, K. Prokes, K. Kiefer, E. Ressouche, A. Paduan-Filho, and M. Kenzelmann, Neutron study of the magnetism in $NiCl_2$-4SC$(NH_2)_2$, J. Phys.: Condens. Matter **25**, 216008 (2013).

[7] A. Paduan-Filho, R. D. Chirico, K. O. Joung, and R. L. Carlin, Field induced magnetic ordering in uniaxial nickel systems: A second example, J. Chem. Phys. **74**, 4103 (1981).

[8] A. Paduan-Filho, X. Gratens, and N. F. Oliveira, High-field magnetization in the quantum spin magnet $NiCl_2$4SC$(NH_2)_2$, J. Appl. Phys. **95**, 7537 (2004).

[9] V. S. Zapf, D. Zocco, B. R. Hansen, M. Jaime, N. Harrison, C. D. Batista, M. Kenzelmann, C. Niedermayer, A. Lacerda, and A. Paduan-Filho, Bose-Einstein Condensation of $S = 1$ Nickel Spin Degrees of Freedom in $NiCl_2$-4SC$(NH_2)_2$, Phys. Rev. Lett. **96**, 077204 (2006).

[10] E. Wulf, D. Hüvonen, R. Schonemann, H. Kuhne, T. Herrmannsdorfer, I. Glavatskyy, S. Gerischer, K. Kiefer, S. Gvasaliya, and A. Zheludev, Critical exponents and intrinsic broadening of the field-induced transition in $NiCl_2$-4SC$(NH_2)_2$, Phys. Rev. B **91**, 014406 (2015)

[11] E. Wulf, D. Hüvonen, J.-W. Kim, A. Paduan-Filho, E. Ressouche, S. Gvasaliya, V. Zapf, and A. Zheludev, Criticality in a disordered quantum antiferromagnet studied by neutron diffraction, Phys. Rev. B **88**, 174418 (2013).

[12] K. Y. Povarov, E. Wulf, D. Hüvonen, J. Ollivier, A. Paduan-Filho, and A. Zheludev, Dynamics of a bond-disordered S = 1 quantum magnet near z = 1 criticality, Phys. Rev. B **92**, 024429 (2015).

[13] K. Y. Povarov, A. Mannig, G. Perren, J. S. Möller, E. Wulf, J. Ollivier, and A. Zheludev, Quantum criticality in a three dimensional spin system at zero field and pressure, Phys. Rev. B **96**, 140414 (2017).

[14] A. Mannig, K. Y. Povarov, J. Ollivier, and A. Zheludev, Spin waves near the edge of halogen substitution induced magnetic order in $Ni(Cl_{1-x}Br_x)_2$-4SC$(NH_2)_2$, Phys. Rev. B **98**, 214419 (2018).

[15] S. A. Zvyagin, J. Wosnitza, A. K. Kolezhuk, V. S. Zapf, M. Jaime, A. Paduan-Filho, V. N. Glazkov, S. S. Sosin, and A. I. Smirnov, Spin dynamics of $NiCl_2$-4SC$(NH_2)_2$ in the field-induced ordered phase, Phys. Rev. B **77**, 092413 (2008).

[16] A. Orlova, R. Blinder, E. Kermarrec, M. Dupont, N. Laflorencie, S. Capponi, H. Mayaffre, C. Berthier, A. Paduan-Filho, and M. Horvatić, Nuclear Magnetic Resonance Reveals Disordered Level-Crossing Physics in the Bose-Glass Regime of the Br-Doped $Ni(Cl_{1-x}Br_x)_2$-4SC$(NH_2)_2$ Compound at a High Magnetic Field, Phys. Rev. Lett. **118**, 067203 (2017).

[17] A. Lopez-Castro and M. R. Truter, The crystal and molecular structure of dichlorotetrakisthioureanickel, $[(NH_2)_2CS]_4NiCl_2$, J. Chem. Soc., 1309 (1963).

[18] S. A. Zvyagin, J. Wosnitza, C. D. Batista, M. Tsukamoto, N. Kawashima, J. Krzystek, V. S. Zapf, M. Jaime, N. F. Oliveira, and A. Paduan-Filho, Magnetic Excitations in the Spin-1 Anisotropic Heisenberg Antiferromagnetic Chain System $NiCl_2$-4SC$(NH_2)_2$, Phys. Rev. Lett. **98**, 047205 (2007).

[19] C. P. Poole, Jr., *Electron Spin Resonance, A Comprehensive Treatise on Experimental Techniques* (Wiley, New York, 1967).

[20] A. G. Gurevich and G. A. Melkov, *Magnetization Oscillations and Waves* (CRC Press, Boca Raton, FL, 1996), Sec. 5.3.

[21] A. Abragam and B. Bleaney, *Electron Paramagnetic Resonance of Transition Ions* (Clarendon Press, Oxford, 1970), Chap. 1, paragraph 5.

[22] S. Al'tshuler and B. Kozyrev, *Electron Paramagnetic Resonance* (Academic Press, New York, 1964).

[23] M. Matsumoto and M. Koga, Longitudinal spin-wave mode near quantum critical point due to uniaxial anisotropy, J. Phys. Soc. Jpn. **76**, 073709 (2007).

[24] Z. Zhang, K. Wierschem, I. Yap, Y. Kato, C. D. Batista, and P. Sengupta, Phase diagram and magnetic excitations of anisotropic spin-one magnets, Phys. Rev. B **87**, 174405 (2013).

[25] A. S. Sherbakov and O. I. Utesov (unpublished).

[26] V. S. Maryasin and M. E. Zhitomirsky, Triangular Antiferromagnet with Nonmagnetic Impurities, Phys. Rev. Lett. **111**, 247201 (2013).

[27] A. I. Smirnov, T. A. Soldatov, O. A. Petrenko, A. Takata, T. Kida, M. Hagiwara, A. Y. Shapiro, and M. E. Zhitomirsky, Order by Quenched Disorder in the Model Triangular Antiferromagnet $RbFe(MoO_4)_2$, Phys. Rev. Lett. **119**, 047204 (2017).

[28] H. Suhl, The theory of ferromagnetic resonance at high signal powers, Phys. Chem. Solids **1**, 209 (1957).

[29] M. I. Kaganov and V. M. Tsukernik, Nonresonance absorption of oscillating magnetic field energy by a ferromagnetic dielectric. II, JETP **11**, 952 (1960).

[30] L. A. Prozorova and A. I. Smirnov, Microwave energy absorption by thermal magnons in the layered antiferromagnet $BaMnF_4$, JETP Lett. **23**, 130 (1976).

[31] H. Yamazaki, Parallel pumping of the brillouin-zone-boundary magnons in a two-dimensional ferromagnet K_2CuF_4, J. Phys. Soc. Jpn. **37**, 667 (1974).

[32] Y. V. Pereverzev and A. V. Stepanov, Two-magnon absorption in low-dimensional biaxial antiferromagnets, Fiz. Nizk. Temp. **3**, 502 (1977).

[33] V. V. Kveder and L. A. Prozorova, Investigation of the beyond-threshold susceptibility in antiferromagnetic $MnCO_3$ and $CsMnF_3$ in parametric excitation of spin waves, JETP Lett. **19**, 353 (1974).